Research Square

Preprints are preliminary reports that have not undergone peer review.
They should not be considered conclusive, used to inform clinical practice,
or referenced by the media as validated information.

Stability and Bifurcation Routes in a Delayed Quadratic Map with Recursive Filtered Memory

Hafidh Khoerul Fata

hafid@lecturer.undip.ac.id

Diponegoro University

Yosephus Decupertino Sumanto

Diponegoro University

Robertus Heri Soelistyo Utomo

Diponegoro University

Research Article

Keywords: delayed quadratic map, recursive filtered memory, Schur–Jury stability, fold bifurcation, flip bifurcation, Neimark–Sacker admissibility

Posted Date: June 25th, 2026

DOI: https://doi.org/10.21203/rs.3.rs-10102939/v1

License: This work is licensed under a Creative Commons Attribution 4.0 International License.
Read Full License

Additional Declarations: No competing interests reported.

Stability and Bifurcation Routes in a Delayed Quadratic Map with Recursive Filtered Memory

Hafidh Khoerul Fata[1*], Yosephus Decupertino Sumanto[1] and Robertus Heri Soelistyo Utomo[1]

[1*]Department of Mathematics, Faculty of Science and Mathematics, Universitas Diponegoro, Semarang, Indonesia.

*Corresponding author(s). E-mail(s): hafid@lecturer.undip.ac.id;
Contributing authors: ydsumanto@lecturer.undip.ac.id;
robertusherisoelisty@lecturer.undip.ac.id;

Abstract

This study investigates a delayed quadratic map with recursive filtered-memory feedback as a smooth discrete-time model for the interaction between direct delay and internal memory filtering. The scalar recurrence is embedded in a three-dimensional polynomial map, allowing the fixed-point branch, Jacobian determinant, invertibility condition, and characteristic polynomial to be derived explicitly. The analysis shows that the delay strength $\boldsymbol{k}$ and filtered-memory strength $\boldsymbol{\eta}$ enter the fixed-point branch through the combined feedback term $\boldsymbol{k} + \boldsymbol{\eta}$, whereas the memory update rate $\boldsymbol{\mu}$ affects the multiplier structure through the Jacobian. Applying the Schur–Jury criterion, we obtain explicit stability thresholds in the fixed-point coordinate. The real-multiplier boundaries are identified as fold and flip thresholds under standard genericity conditions, and their coincidence gives a fold–flip degeneracy. The third Schur–Jury boundary is shown to be only a complex-pair candidate: it becomes admissible as a non-real unit-circle crossing only under sign-dependent conditions on the filtered-memory feedback. Numerical continuations, Lyapunov spectra, Kaplan–Yorke dimension, phase-space projections, and parameter-plane scans support the analytical separation between the fold and flip route and the admissible complex-pair route.

Keywords: delayed quadratic map, recursive filtered memory, Schur–Jury stability, fold bifurcation, flip bifurcation, Neimark–Sacker admissibility

MSC Classification: 37G35 , 39A28 , 37M20 , 37C70

1 Introduction

Nonlinear discrete maps provide a concise framework for studying stability transitions, bifurcations, chaos, and post-critical dynamics in discrete-time dynamical systems [1, 2]. Classical examples, such as the logistic map, show that even one-dimensional deterministic recurrences can generate period-doubling cascades, chaotic dynamics, and sensitive dependence on initial conditions [1]. Quadratic maps and their variants have also been used to analyze memory effects and non-Markovian feedback mechanisms in discrete dynamical systems [2]. Dependence on past states enriches these dynamics by increasing the effective dimension of the recurrence and producing higher order discrete-time systems.

Delayed and second-order maps have been studied in several related contexts. Delayed quadratic maps, including recurrences involving past states such as $x_{t-\tau}$, arise naturally in the study of memory effects in discrete dynamical systems [2]. More general second-order rational or quadratic difference equations may exhibit periodic solutions, chaotic dynamics, and local bifurcations, including fold, flip, and Neimark–Sacker bifurcations [3–5]. Related second-order and higher-dimensional maps from applied models may also display degenerate or higher-codimension phenomena, such as generalized flips and Chenciner-type bifurcations [6]. These results indicate that delayed dependence can substantially modify the multiplier structure and the postcritical dynamics of nonlinear maps.

Memory can enter a discrete map in multiple ways. A delay maintains an old state as part of the next update. In contrast, a filter updates an auxiliary state that summarizes the recent history. This difference is important because the filter is not applied after the orbit is generated; it participates in the feedback loop that generates the next iterate. Studies on logistic-type maps with first-order, weighted, and geometric memory show that these memory terms can widen stability intervals, shift bifurcation diagrams, and affect the boundedness of trajectories [7–10]. Fractional-type maps provide another form of memory, where past states enter through long power-law-weighted histories [11, 12]. Here, we use the recursive filtered form so that the delayed coordinate and internal memory response can be separated explicitly.

Delayed and filtered feedback also appears across several modeling contexts. In population dynamics, difference-delay equations represent lagged regulatory effects and oscillatory responses [13]. In economic dynamics, second-order difference equations and lagged adjustment mechanisms appear in the Samuelson multiplier–accelerator model and its later bifurcation-theoretic interpretations [14, 15]. In control theory, delayed feedback and feedback gains are standard mechanisms for modifying stability and controlling nonlinear dynamics [16, 17]. These examples motivate the use of delay and filtering as generic feedback mechanisms rather than application-specific assumptions.

The local bifurcation structure of the fixed points provides the first analytical view of the interaction between the delay and filtering. For discrete maps, fixed-point stability is lost through multiplier crossings of the unit circle, typically through fold, flip, or Neimark–Sacker mechanisms [18]. In delayed or higher-dimensional maps, these mechanisms may interact with additional memory-induced directions in nontrivial ways [6, 19, 20]. A rigorous interpretation of a unit-circle boundary requires more than locating an equality in the stability condition. Simplicity, transversality,

non-resonance, and nonlinear non-degeneracy conditions are required to identify the corresponding local bifurcation mechanism [18, 20]. For the present model, the relevant question is how the quadratic term, delayed coordinate, filtered memory strength, and memory update rate enter the multiplier conditions. The third Jury boundary is particularly delicate. Although it is obtained from the Schur–Jury inequalities, it does not imply a Neimark–Sacker bifurcation. It is still necessary to determine whether the corresponding multipliers form a genuinely non-real pair on the unit circle.

The fixed-point thresholds determine where local stability is lost, but they do not describe the orbit after leaving the fixed-point regime. After a real multiplier or admissible complex pair crossing, the map may show periodic windows, chaotic bands, or invariant curve dynamics. Memory-modified logistic and quadratic-type maps indicate that memory can change the observed bifurcation route [9, 21]. Therefore, the analytical thresholds are complemented here by bifurcation diagrams, Lyapunov spectra, Kaplan–Yorke dimension, phase-space projections, and parameter-plane scans.

A systematic explicit characterization of a smooth quadratic map that combines quadratic nonlinearity, one-step delay, and recursive filtered-memory feedback remains underdeveloped. Related studies have treated delayed quadratic maps, second-order difference equations, and memory-modified logistic-type maps in different forms; however, the coupling of delay and recursive filtering in a single polynomial map has received less attention. In the present setting, there are no singularities in the denominator. Therefore, the stability loss and local bifurcation thresholds can be traced directly to the interaction among the quadratic nonlinearity, delayed coordinate, and filtered-memory state.

This study analyzes a delayed quadratic map augmented with recursive filtered-memory feedback. The recurrence is embedded into a smooth three-dimensional polynomial map so that the fixed-point branches, Jacobian determinant, invertibility properties, and characteristic polynomial can be obtained explicitly. The local stability problem is then reduced to the multipliers of the embedded maps. Applying the Schur–Jury criterion to the characteristic polynomial yields stability inequalities that can be written directly in the fixed-point coordinate x^* or, equivalently, in terms of the local quadratic slope. This reduction separates the real-multiplier boundaries from the complex pair boundary. The former provides the fold and flip thresholds, whereas the latter requires an additional admissibility test before it can be interpreted as a genuine fixed-point Neimark–Sacker threshold.

The contribution of this study is to make this separation explicit. The delayed quadratic recurrence with recursive filtered memory is first written as a smooth three-dimensional polynomial map, from which the fixed-point branch, Jacobian determinant, invertibility, and characteristic polynomial are obtained. The Schur–Jury criterion is then reduced to closed-form stability inequalities in x^*. These inequalities identify the real-multiplier fold and flip thresholds under explicit genericity conditions, whereas the third Schur–Jury boundary is treated separately through an admissibility condition for the complex pair. Finally, numerical continuations and parameter-plane scans are used to examine how the admissible real-multiplier and complex-pair routes organize different post-critical attractor transitions.

The remainder of this paper is organized as follows. Section 2 introduces the model and its fundamental properties. Section 3 presents a fixed-point stability analysis. Section 4 derives the local bifurcation criteria and admissibility conditions for the complex-pair boundary. Section 5 presents the numerical validation and attractor transition scenarios. Section 6 concludes the paper.

2 Model formulation and basic properties

We consider the delayed quadratic recurrence with recursive first-order filtered-memory feedback

$$\begin{aligned} x_{n+1} &= c - ax_n^2 + kx_{n-1} + \eta z_n, \\ z_{n+1} &= (1-\mu)z_n + \mu x_n, \end{aligned} \tag{1}$$

where $a > 0$, $c, k, \eta \in \mathbb{R}$, and $0 < \mu < 1$. The parameter k measures the explicit one-step delayed feedback, η measures the strength of the filtered memory feedback, and μ is the memory update rate.

Variable z_n is not an independent forcing term. Iterating the second equation of (1) gives

$$z_n = (1-\mu)^n z_0 + \mu \sum_{j=0}^{n-1} (1-\mu)^j x_{n-1-j}. \tag{2}$$

Thus, z_n is an exponentially weighted record of the past states of x. Small values of μ produce slow memory updating, whereas values of μ close to one cause the filter to respond mainly to the most recent state.

Because $a > 0$, the quadratic coefficient can be removed by the invertible linear scaling $X_n = ax_n$, $Z_n = az_n$, and $C = ac$. This normalization does not change the qualitative stability or bifurcation structure because it is induced by an invertible linear change in the variables and parameters. After multiplying the first equation in (1) by a and renaming (X, Z, C) as (x, z, c), we obtain

$$\begin{aligned} x_{n+1} &= c - x_n^2 + kx_{n-1} + \eta z_n, \\ z_{n+1} &= (1-\mu)z_n + \mu x_n. \end{aligned} \tag{3}$$

All analytical results below are stated for the normalized system in (3). The corresponding statements for (1) are recovered through the inverse scaling $x = X/a$, $z = Z/a$, and $c = C/a$.

Setting $y_n = x_{n-1}$, system (3) is embedded as the three-dimensional polynomial map

$$F(x, y, z) = \big(c - x^2 + ky + \eta z,\ x,\ (1-\mu)z + \mu x\big). \tag{4}$$

The delay-only case corresponds to $\eta = 0$, the filter-only case to $k = 0$, and the coupled delay–filter case to $k\eta \neq 0$. This embedding is useful because the local dynamics near a fixed point can be studied using the multipliers of a smooth map on $\mathbb{R}^3$.

2.1 Structural properties

The Jacobian matrix of (4) is

$$DF(x,y,z) = \begin{pmatrix} -2x & k & \eta \\ 1 & 0 & 0 \\ \mu & 0 & 1-\mu \end{pmatrix}. \tag{5}$$

Its determinant is independent of the phase-space point as follows:

$$\det DF = -k(1-\mu). \tag{6}$$

Hence, the explicit delayed-feedback coefficient k determines whether the embedded map is locally invertible.

Proposition 1 (Global invertibility) *Assume $0 < \mu < 1$. The map F is a global diffeomorphism on $\mathbb{R}^3$ if and only if $k \neq 0$. In this case, if $(U,V,W) = F(x,y,z)$, then*

$$x = V, \qquad z = \frac{W-\mu V}{1-\mu}, \qquad y = \frac{U - c + V^2 - \eta\left(\dfrac{W-\mu V}{1-\mu}\right)}{k}. \tag{7}$$

Proof If $k \neq 0$, the second and third components of $F(x,y,z) = (U,V,W)$ give $x = V$ and $z = (W-\mu V)/(1-\mu)$. Substituting these expressions into $U = c - V^2 + ky + \eta z$ yields (7). Hence, the inverse exists and is smooth on all of $\mathbb{R}^3$. If $k = 0$, the map is independent of y. Thus, two points with the same (x,z) and different y-coordinates have the same image; therefore, F is not injective. Therefore F is a global diffeomorphism if and only if $k \neq 0$. □

For $k \neq 0$, the map is orientation-reversing when $k > 0$ and orientation-preserving when $k < 0$. The constant Jacobian determinant shows that the volumes are multiplied by $|k(1-\mu)|$ under one iteration. Hence, the map is volume contracting when $|k(1-\mu)| < 1$. However, this volume contraction does not imply the existence of a bounded absorbing set for all initial conditions.

Because the first component contains the term $-x^2$, sufficiently large negative amplitudes are driven further toward $-\infty$. The following elementary cone estimate distinguishes bounded dynamics from escaping the trajectories.

Lemma 2 (Escape cone at negative amplitudes) *Let $K = |k| + |\eta|$. Choose $R_{\mathrm{esc}} > 0$ such that*

$$R_{\mathrm{esc}} > \frac{K+2}{2}, \qquad R_{\mathrm{esc}}^2 - (K+2)R_{\mathrm{esc}} - |c| > 0. \tag{8}$$

If, for some n, $x_n \leq -R_{\mathrm{esc}}$, $|y_n| \leq |x_n|$, and $|z_n| \leq |x_n|$, then the forward orbit escapes to infinity and $x_m \to -\infty$ as $m \to \infty$.

Proof Set $s = |x_n|$. Since $s \geq R_{\mathrm{esc}}$, the first component of (4) gives $x_{n+1} \leq |c| - s^2 + Ks$. By (8), one has $|c| - s^2 + Ks < -2s$. Therefore $x_{n+1} < -2s < 0$, and hence $|x_{n+1}| > 2|x_n|$. Moreover, $|y_{n+1}| = |x_n| < |x_{n+1}|$, while $|z_{n+1}| \leq (1-\mu)|z_n| + \mu|x_n| \leq |x_n| < |x_{n+1}|$. Thus, the same cone condition holds at the next iteration with a larger value of $|x|$. Repeating the argument gives $x_m \to -\infty$. □

Lemma 2 shows that no bounded subset of $\mathbb{R}^3$ can absorb all forward orbits. Therefore, the bounded invariant sets considered below are conditional on the parameter values and the chosen initial conditions.

2.2 Fixed-point branches

The fixed points of (4) have a particularly simple structure. The second and third components of $F(p^*) = p^*$ imply $y^* = x^*$ and $z^* = x^*$. Hence, every fixed point lies on the diagonal.

Proposition 3 (Fixed-point branches) *The fixed points of (4) are diagonal point $p^* = (x^*, x^*, x^*)$, where x^* satisfies*

$$(x^*)^2 + (1 - k - \eta)x^* - c = 0. \tag{9}$$

Equivalently, the fixed-point branch is parametrized by

$$c = c(x^*) = (x^*)^2 + (1 - k - \eta)x^*. \tag{10}$$

Let $\Delta = (1-k-\eta)^2 + 4c$. If $\Delta > 0$, there are two real fixed points $p^*_\pm = (x^*_\pm, x^*_\pm, x^*_\pm)$, where

$$x^*_\pm = \frac{-(1-k-\eta) \pm \sqrt{\Delta}}{2}. \tag{11}$$

If $\Delta = 0$, the two fixed-point branches meet at

$$x^*_F = \frac{k+\eta-1}{2}, \qquad c_F = -\frac{(1-k-\eta)^2}{4}. \tag{12}$$

If $\Delta < 0$, no real fixed point exists.

Proof Substituting $p^* = (x^*, y^*, z^*)$ into $F(p^*) = p^*$, the second component gives $y^* = x^*$. The third component gives $z^* = (1-\mu)z^* + \mu x^*$, and because $0 < \mu < 1$, this yields $z^* = x^*$. The first component then reduces to (9). The parametrization (10), the two roots (11), and the coalescence point (12) follow directly from this quadratic formula. □

The fixed-point location depends on k and η through the combined feedback term $1 - k - \eta$, whereas μ does not enter (9). Therefore, the memory update rate affects the local dynamics through the Jacobian and multipliers, not through the location of the fixed-point branch.

The branch geometry follows from

$$\frac{dc}{dx^*} = 2x^* + 1 - k - \eta = 2(x^* - x^*_F). \tag{13}$$

Thus, x_F^* is the turning coordinate of the fixed-point branch. Since $\Delta = 4(c - c_F)$, for $c > c_F$ we may write

$$x_\pm^* = x_F^* \pm \sqrt{c - c_F}, \tag{14}$$

and consequently $x_-^* < x_F^* < x_+^*$. The coordinate x_F^* is introduced here only as the turning point of the fixed point branch. Its multiplier interpretation is established in Sections 3 and 4.

The preceding reduction shows that the local dynamics near a fixed point can be parameterized by the scalar coordinate x^*. The next section uses this coordinate to express the Schur–Jury stability conditions and the associated unit-circle thresholds.

3 Fixed-point stability

Let $p^* = (x^*, x^*, x^*)$ be a fixed point of (4). By Proposition 3, the fixed-point branch is parameterized by x^* through $c = c(x^*)$. The local dynamics near p^* is determined by the multipliers of the Jacobian matrix $J_* = DF(p^*)$, namely

$$J_* = \begin{pmatrix} -2x^* & k & \eta \\ 1 & 0 & 0 \\ \mu & 0 & 1-\mu \end{pmatrix}. \tag{15}$$

A direct computation gives the characteristic polynomial

$$P(\lambda; x^*) = \lambda^3 - (1 - \mu - 2x^*)\lambda^2 + \big[-2(1-\mu)x^* - \eta\mu - k\big]\lambda + k(1-\mu). \tag{16}$$

Equivalently, writing $P(\lambda; x^*) = \lambda^3 + a_1\lambda^2 + a_2\lambda + a_3$, the coefficients are

$$a_1 = 2x^* + \mu - 1, \qquad a_2 = -2(1-\mu)x^* - \eta\mu - k, \qquad a_3 = k(1-\mu). \tag{17}$$

For a monic cubic polynomial $\lambda^3 + a_1\lambda^2 + a_2\lambda + a_3$, the Schur–Jury criterion states that all roots lie strictly inside the unit disk if and only if

$$\begin{aligned} 1 + a_1 + a_2 + a_3 &> 0, \\ 1 - a_1 + a_2 - a_3 &> 0, \\ 1 - a_2 + a_1 a_3 - a_3^2 &> 0, \\ |a_3| &< 1. \end{aligned} \tag{18}$$

The following lemma reduces these four inequalities to explicit conditions in the fixed-point coordinate x^*.

Lemma 4 (Schur–Jury reduction) *For the characteristic polynomial* (16)*, the Schur–Jury quantities in* (18) *satisfy*

$$\begin{aligned} 1 + a_1 + a_2 + a_3 &= \mu(1 + 2x^* - \eta - k), \\ 1 - a_1 + a_2 - a_3 &= 2(2-\mu)(x^*_{PD} - x^*), \\ 1 - a_2 + a_1 a_3 - a_3^2 &= H(x^*), \\ |a_3| &= |k(1-\mu)|, \end{aligned} \tag{19}$$

where

$$x^*_F = \frac{k + \eta - 1}{2}, \qquad x^*_{PD} = \frac{(2-\mu)(1-k) - \mu\eta}{2(2-\mu)}, \tag{20}$$

and

$$H(x^*) = (1+k)\big[1 - k(1-\mu)^2 + 2(1-\mu)x^*\big] + \eta\mu. \tag{21}$$

Proof Substitution of (17) into the four Schur–Jury quantities gives the identities directly. In particular, $1 + a_1 + a_2 + a_3 = \mu(1 + 2x^* - \eta - k) = 2\mu(x^* - x^*_F)$, and $1 - a_1 + a_2 - a_3 = 2(2-\mu)(x^*_{PD} - x^*)$. The third identity follows by collecting terms in x^*, and the last one follows from $a_3 = k(1-\mu)$. □

The coordinate x^*_F is the turning point of the fixed-point branch introduced in Section 2. The coordinate x^*_{PD} is the real multiplier candidate at which $P(-1; x^*) = 0$. For any threshold coordinate x^*_T, we write $c_T = c(x^*_T)$. In particular, $c_{PD} = c(x^*_{PD})$.

The third Schur–Jury boundary is determined by $H(x^*) = 0$. If $k \neq -1$, this boundary can be written as $x^* = x^*_C$, where

$$x^*_C = -\frac{1}{2}\left[\frac{1 - k(1-\mu)^2}{1-\mu} + \frac{\eta\mu}{(1+k)(1-\mu)}\right]. \tag{22}$$

The subscript C indicates the complex pair candidate threshold. It is not called a Neimark–Sacker threshold at this stage because the equality $H(x^*) = 0$ alone does not guarantee a genuinely admissible complex-pair crossing. This admissibility issue is addressed in Section 4.

Proposition 5 (Fixed-point stability) *Let $p^* = (x^*, x^*, x^*)$ be a fixed point of* (4)*. Then p^* is locally asymptotically stable if and only if*

$$|k(1-\mu)| < 1, \qquad x^* > x^*_F, \qquad x^* < x^*_{PD}, \qquad H(x^*) > 0. \tag{23}$$

Equivalently, if $k > -1$, then p^* is locally asymptotically stable if and only if

$$|k(1-\mu)| < 1, \qquad \max\{x^*_F, x^*_C\} < x^* < x^*_{PD}. \tag{24}$$

If $k = -1$, then p^* is locally asymptotically stable if and only if

$$|k(1-\mu)| < 1, \qquad \eta > 0, \qquad x^*_F < x^* < x^*_{PD}. \tag{25}$$

If $k < -1$, then p^* is locally asymptotically stable if and only if

$$|k(1-\mu)| < 1, \qquad x^*_F < x^* < \min\{x^*_{PD}, x^*_C\}. \tag{26}$$

Proof According to the Schur–Jury criterion, local asymptotic stability is equivalent to the four inequalities in (18). Lemma 4 shows that these inequalities are precisely the four conditions in (23), since $0 < \mu < 1$ and $2 - \mu > 0$.

It remains to rewrite the inequality $H(x^*) > 0$. When $k > -1$, the coefficient of x^* in H is positive, so $H(x^*) > 0$ is equivalent to $x^* > x_C^*$. When $k < -1$, the coefficient of x^* in H is negative, so $H(x^*) > 0$ is equivalent to $x^* < x_C^*$. When $k = -1$, one has $H(x^*) = \eta\mu$, so $H(x^*) > 0$ is equivalent to $\eta > 0$. This proves the three cases. □

The stability conditions in Proposition 5 are expressed entirely in terms of the fixed-point coordinate x^*. Along a fixed-point branch, the corresponding parameter thresholds are obtained by the branch map $c = c(x^*)$. Thus, $c_F = c(x_F^*)$, $c_{PD} = c(x_{PD}^*)$, and, whenever $k \neq -1$, $c_C = c(x_C^*)$.

The most relevant regime for positive delay and positive filtered feedback is particularly simple.

Corollary 6 (Positive delay–filter feedback) *Assume* $0 < k < 1$, $\eta \geq 0$, *and* $0 < \mu < 1$. *Then* $|k(1-\mu)| < 1$, *and the third Schur–Jury inequality is automatically satisfied for all* $x^* \geq x_F^*$. *Consequently, a fixed point is locally asymptotically stable if and only if*

$$x_F^* < x^* < x_{PD}^*. \tag{27}$$

This stability interval is nonempty if and only if

$$\eta < (2-\mu)(1-k). \tag{28}$$

Proof Since $0 < k < 1$ and $0 < \mu < 1$, one has $|k(1-\mu)| < 1$. Moreover, H increases in x^* because its slope is $2(1+k)(1-\mu) > 0$. At the fold coordinate,

$$H(x_F^*) = (1+k)\big[\mu + k\mu(1-\mu) + (1-\mu)\eta\big] + \eta\mu, \tag{29}$$

which is positive for $0 < k < 1$ and $\eta \geq 0$. Hence $H(x^*) > 0$ for all $x^* \geq x_F^*$. Proposition 5 then reduces the stability condition to (27). Finally, $x_F^* < x_{PD}^*$ is equivalent to $\eta < (2 - \mu)(1-k)$, which proves (28). □

Corollary 6 shows that in the positive delay–filter regime, the third Schur–Jury boundary does not bound the stable part of the upper fixed-point branch. For $c > c_F$, the lower branch $x_-^* < x_F^*$ fails the first Schur–Jury inequality and is therefore unstable. The upper branch $x_+^* > x_F^*$ is stable precisely while $x_+^* < x_{PD}^*$, or equivalently while $c_F < c < c_{PD}$, provided that (28) holds. Thus, in this parameter regime, the first loss of stability along the upper branch is organized by the real multiplier boundary $P(-1; x^*) = 0$. The generic flip interpretation of this boundary is established in Section 4.

When the signs of k and η are allowed to vary, the third Schur–Jury boundary may enter the relevant fixed-point branch. This is the regime in which complex pair admissibility becomes important. Therefore, the next section interprets the real-multiplier thresholds and complex-pair candidate threshold as local bifurcation boundaries under the appropriate genericity and admissibility conditions.

4 Local bifurcation criteria

Throughout this section, k, η, and μ are regarded as fixed parameters, with $0 < \mu < 1$, whereas c is used as the continuation parameter along the fixed-point branch $c = c(x^*)$. The equality cases in the Schur–Jury conditions identify candidate unit-circle crossings. The purpose of this section is to determine when these candidate crossings correspond to genuine, local bifurcations.

Because the nonlinearity of F appears only in the first component, the only nonzero second derivative is generated by the term $-x^2$. Hence the symmetric bilinear part of F is

$$B(u, v) = (-2u_1v_1, 0, 0)^T, \tag{30}$$

and all the third-order derivatives vanish.

4.1 Fold bifurcation

At the branch turning point $x^* = x_F^*$, the characteristic polynomial satisfies $P(1; x_F^*) = 0$. Thus, $\lambda = 1$ is a multiplier of $J_* = DF(p^*)$. The following lemma records the algebraic quantities required for the fold non-degeneracy condition.

Lemma 7 (Fold eigenvectors and non-degeneracy) *At $x^* = x_F^*$, a right eigenvector associated with $\lambda = 1$ is*

$$q_F = (1, 1, 1)^T. \tag{31}$$

A corresponding left eigenvector is proportional to

$$\widetilde{p}_F = \left(1, k, \frac{\eta}{\mu}\right)^T. \tag{32}$$

Moreover,

$$\langle \widetilde{p}_F, q_F \rangle = 1 + k + \frac{\eta}{\mu} = \frac{\mu(1 + k) + \eta}{\mu}. \tag{33}$$

Therefore the multiplier $\lambda = 1$ is simple whenever

$$\mu(1 + k) + \eta \neq 0. \tag{34}$$

Under this condition, after normalizing $p_F = \widetilde{p}_F / \langle \widetilde{p}_F, q_F \rangle$, one has

$$\langle p_F, F_c \rangle = \frac{1}{1 + k + \eta/\mu}, \qquad \langle p_F, B(q_F, q_F) \rangle = -\frac{2}{1 + k + \eta/\mu}. \tag{35}$$

Both quantities were nonzero.

Proof At $x^* = x_F^*$, one has $-2x_F^* = 1 - k - \eta$. Substituting this identity into $J_* q_F$ yields $J_* q_F = q_F$. The left eigenvector relation $J_*^T \widetilde{p}_F = \widetilde{p}_F$ is verified directly from (32). The normalization factor is given by (33). Since $F_c = (1, 0, 0)^T$ and $B(q_F, q_F) = (-2, 0, 0)^T$, the two identities in (35) follow immediately. □

Proposition 8 (Generic fold bifurcation) *Assume that $x^* = x_F^*$, that the remaining multipliers of J_* are not on the unit circle, and that $\mu(1 + k) + \eta \neq 0$. Then, the fixed point undergoes a generic fold bifurcation at $c = c_F$.*

Proof By Lemma 7, the multiplier $\lambda = 1$ is a simple multiplier. The unfolding coefficient $\langle p_F, F_c \rangle$ is nonzero; therefore, the parameter c unfolds the fixed-point equation transversally. The quadratic coefficient $\langle p_F, B(q_F, q_F) \rangle$ is also non-zero. Together with the hyperbolicity of the remaining multipliers, these are the standard non-degeneracy conditions for the fold bifurcation of maps. □

4.2 Flip bifurcation

At the coordinate $x^* = x^*_{PD}$, one has $P(-1; x^*_{PD}) = 0$. Hence, $\lambda = -1$ is a multiplier. Two algebraic quantities determine the simplicity of this multiplier and its separation from the fold point:

$$D_{\text{simp}} = 1 + k + \frac{\eta\mu}{(2-\mu)^2}, \qquad D_{\text{sep}} = (2-\mu)(1-k) - \eta. \tag{36}$$

Lemma 9 (Simplicity and crossing at the flip threshold) *At $x^* = x^*_{PD}$, the multiplier $\lambda = -1$ is simple if and only if $D_{\text{simp}} \neq 0$. Moreover,*

$$\frac{\partial P}{\partial \lambda}(-1; x^*_{PD}) = (2-\mu) D_{\text{simp}}, \tag{37}$$

and

$$\left.\frac{dc}{dx^*}\right|_{x^* = x^*_{PD}} = \frac{2 D_{\text{sep}}}{2-\mu}. \tag{38}$$

Consequently, if $D_{\text{simp}} D_{\text{sep}} \neq 0$, then the -1-multiplier crossing is transversal with respect to c, with

$$\left.\frac{d\lambda}{dc}\right|_{c = c_{PD}} = -\frac{2-\mu}{D_{\text{simp}} D_{\text{sep}}}. \tag{39}$$

Proof The identity (37) follows by differentiating (16) with respect to λ and substituting $\lambda = -1$ and $x^* = x^*_{PD}$. Hence, the root -1 is simple precisely when $D_{\text{simp}} \neq 0$. The branch derivative (38) follows from $dc/dx^* = 2(x^* - x^*_F)$ and the explicit expressions for x^*_F and x^*_{PD}. Finally, differentiating $P(\lambda(x^*); x^*) = 0$ yields $d\lambda/dx^* = -2/D_{\text{simp}}$ at $x^* = x^*_{PD}$. Dividing by dc/dx^* yields (39). □

A right eigenvector for $\lambda = -1$ at $x^* = x^*_{PD}$ is

$$q_{PD} = \left(1, -1, -\frac{\mu}{2-\mu}\right)^T, \tag{40}$$

and a corresponding left eigenvector is proportional to

$$\widetilde{p}_{PD} = \left(1, -k, -\frac{\eta}{2-\mu}\right)^T. \tag{41}$$

Their inner product is $\langle \widetilde{p}_{PD}, q_{PD} \rangle = D_{\text{simp}}$. Hence, when $D_{\text{simp}} \neq 0$, we normalize $p_{PD} = \widetilde{p}_{PD} / D_{\text{simp}}$.

The quadratic term also yields a nonzero flip coefficient whenever the flip threshold is separated from the fold point. Indeed, let h_{PD} be the solution of $(J_* - I)h_{PD} = B(q_{PD}, q_{PD})$ at $x^* = x^*_{PD}$. If $D_{\text{sep}} \neq 0$, then

$$h_{PD} = \frac{2-\mu}{D_{\text{sep}}}(1,1,1)^T, \tag{42}$$

and therefore

$$\langle p_{PD}, B(q_{PD}, h_{PD})\rangle = -\frac{2(2-\mu)}{D_{\text{sep}} D_{\text{simp}}}. \tag{43}$$

This projected quadratic term is nonzero whenever $D_{\text{sep}} D_{\text{simp}} \neq 0$.

Proposition 10 (Generic flip bifurcation) *Assume that $x^* = x^*_{PD}$, that the remaining multipliers of J_* are not on the unit circle, and that*

$$D_{\text{simp}} D_{\text{sep}} \neq 0. \tag{44}$$

Then, the fixed point undergoes a generic flip bifurcation at $c = c_{PD}$.

Proof The condition $D_{\text{simp}} \neq 0$ makes the multiplier -1 simple and straightforward. The condition $D_{\text{sep}} \neq 0$ separates the flip point from the fold turning point and makes $c = c(x^*)$ a regular continuation parameter at x^*_{PD}. Lemma 9 gives a nonzero crossing speed with respect to c, and (43) gives a nonzero nonlinear coefficient. Together with the hyperbolicity of the remaining multipliers, these are the standard non-degeneracy conditions for a flip bifurcation of maps. □

The equality $D_{\text{sep}} = 0$ is equivalent to

$$\eta = (2-\mu)(1-k). \tag{45}$$

At this locus, $x^*_{PD} = x^*_F$, so the fold and flip thresholds coincide. Thus, (45) is the fold–flip degeneracy of the fixed-point thresholds. A full two-parameter unfolding of this degeneracy was not pursued here.

4.3 Complex-pair boundary and Neimark–Sacker admissibility

The third Schur–Jury boundary is given by $H(x^*) = 0$. When $k \neq -1$, it is represented by the candidate coordinate x^*_C defined in Eq. (22). At this boundary, the characteristic polynomial can be written in the form

$$P(\lambda; x^*_C) = (\lambda^2 - 2\cos\theta\,\lambda + 1)(\lambda - \nu), \tag{46}$$

where

$$\nu = -k(1-\mu), \qquad \cos\theta = \frac{1}{2}\left(\frac{1}{1-\mu} + 1 - \mu\right) + \frac{\eta\mu}{2(1+k)(1-\mu)}. \tag{47}$$

The boundary $H(x^*) = 0$ corresponds to a non-real unit-modulus pair only if $-1 < \cos\theta < 1$. This provides an explicit admissibility condition for the filtered-memory feedback strength.

Proposition 11 (Admissibility of the complex-pair boundary) *Assume $0 < \mu < 1$ and $k \neq -1$. The third Schur–Jury boundary is admissible as a non-real complex-pair unit-circle boundary if and only if the following conditions are satisfied:*

If $k > -1$, then

$$-\frac{(1+k)(2-\mu)^2}{\mu} < \eta < -\mu(1+k). \tag{48}$$

If $k < -1$, then

$$-\mu(1+k) < \eta < -\frac{(1+k)(2-\mu)^2}{\mu}. \tag{49}$$

Proof The pair in (46) is non-real and lies on the unit circle exactly when $-1 < \cos\theta < 1$. Substituting (47) into this inequality gives

$$-1 < \frac{1}{2}\left(\frac{1}{1-\mu} + 1 - \mu\right) + \frac{\eta\mu}{2(1+k)(1-\mu)} < 1. \tag{50}$$

Solving this double inequality for η gives (48) when $k > -1$, because the coefficient of η is positive. If $k < -1$, the coefficient of η is negative and the inequalities reverse, giving (49). □

Corollary 12 (Exclusion in the positive delay–filter regime) *Assume $0 < k < 1$, $\eta \geq 0$, and $0 < \mu < 1$. Then the third Schur–Jury boundary cannot represent a non-real unit-circle crossing. Hence the positive delay–filter regime admits no Neimark–Sacker bifurcation from the fixed point.*

Proof If $0 < k < 1$, then $k > -1$. By Proposition 11, admissibility would require $\eta < -\mu(1+k) < 0$, which contradicts $\eta \geq 0$. □

The admissibility of the complex pair is still not the whole Neimark–Sacker verification. Once the multipliers lie on the unit circle, one must also exclude low-order resonances and check the usual transversality and non-degeneracy conditions. We denote by ℓ_1 the first Lyapunov coefficient of the two-dimensional center dynamics at the complex pair boundary, which is computed from the Neimark–Sacker normal form for maps.

Proposition 13 (Generic Neimark–Sacker criterion) *Assume $k \neq -1$, $x^* = x^*_C$, and $|k(1-\mu)| < 1$. Suppose further that the admissibility condition in Proposition 11 holds, so that $\lambda_{1,2} = e^{\pm i\theta}$ with $0 < \theta < \pi$, and that*

$$x^*_C \neq x^*_F, \qquad e^{im\theta} \neq 1 \quad \text{for } m = 1, 2, 3, 4, \qquad \ell_1 \neq 0. \tag{51}$$

Then, the fixed point undergoes a generic Neimark–Sacker bifurcation at $c = c_C$.

Proof The condition $|k(1-\mu)| < 1$ yields $|\nu| < 1$, so the third multiplier is strictly inside the unit disk. The admissibility condition yields a non-real unit-modulus pair $e^{\pm i\theta}$.Because $H'(x^*) = 2(1+k)(1-\mu) \neq 0$ for $k \neq -1$, and $x_C^* \neq x_F^*$ makes $dc/dx^* \neq 0$ at the crossing, the complex-pair boundary is crossed transversally along the c-continuation line. The non-resonance conditions exclude the low-order resonances, and $\ell_1 \neq 0$ provides the standard nonlinear non-degeneracy condition. Hence, the boundary is a generic Neimark–Sacker bifurcation point. □

The preceding criteria separate the real-multiplier and complex-pair routes. In the positive delay–filter regime, the admissible fixed-point stability window terminates at the flip threshold. When the delayed and filtered memory feedbacks have competing signs, the complex pair boundary may become admissible and may organize invariant curve dynamics after the loss of fixed-point stability.

5 Numerical validation and attractor transitions

The analytical results above separate two local routes from fixed-point stability: the real-multiplier route, organized by the fold and flip thresholds, and the complex-pair route, organized by the admissible third Schur–Jury boundary. The numerical experiments in this section are not intended to catalogue all the possible bounded invariant sets. Instead, they illustrate how the explicit thresholds derived in Sections 3 and 4 organize the observed attractor transitions of the delayed filtered memory map.

All computations were performed on the embedded map (4). Unless otherwise stated, the one-parameter sweeps were computed using forward continuation. After discarding a transient at one parameter value, the last iteration was used as the initial condition for the next parameter value. For each parameter value, the first N_{trans} iterations were discarded, and the next N_{keep} iterations were retained for plotting and diagnostics. A trajectory was declared escaping when $\max\{|x_n|, |y_n|, |z_n|\}$ exceeded the prescribed numerical-escape threshold. Lyapunov exponents were computed along the variational equation $v_{n+1} = DF(x_n, y_n, z_n)v_n$ using QR reorthonormalization, following standard algorithms for Lyapunov-spectrum computation in smooth dynamical systems [22–24]. The Kaplan–Yorke dimension was computed from the ordered Lyapunov exponents $\Lambda_1 \geq \Lambda_2 \geq \Lambda_3$ [25]. If all the Lyapunov exponents are negative, we set $D_{KY} = 0$. Otherwise,

$$D_{KY} = j + \frac{\sum_{i=1}^{j} \Lambda_i}{|\Lambda_{j+1}|}, \qquad \sum_{i=1}^{j} \Lambda_i \geq 0, \quad \sum_{i=1}^{j+1} \Lambda_i < 0. \tag{52}$$

Periodic windows, chaotic bands, and invariant-curve-like dynamics were identified from the combined information supplied by bifurcation diagrams, Lyapunov spectra, phase-space projections, and parameter-plane scans. The parameter values, continuation ranges, iteration lengths, and escape conventions used for each experiment are reported in the corresponding captions.

We first consider the positive delay–filter regime $(k, \eta, \mu) = (0.35, 0.25, 0.45)$. In this case, Corollary 6 gives the fixed-point stability window $x_F^* < x^* < x_{PD}^*$, whereas Corollary 12 excludes a fixed-point Neimark–Sacker route. Thus, the upper fixed-point

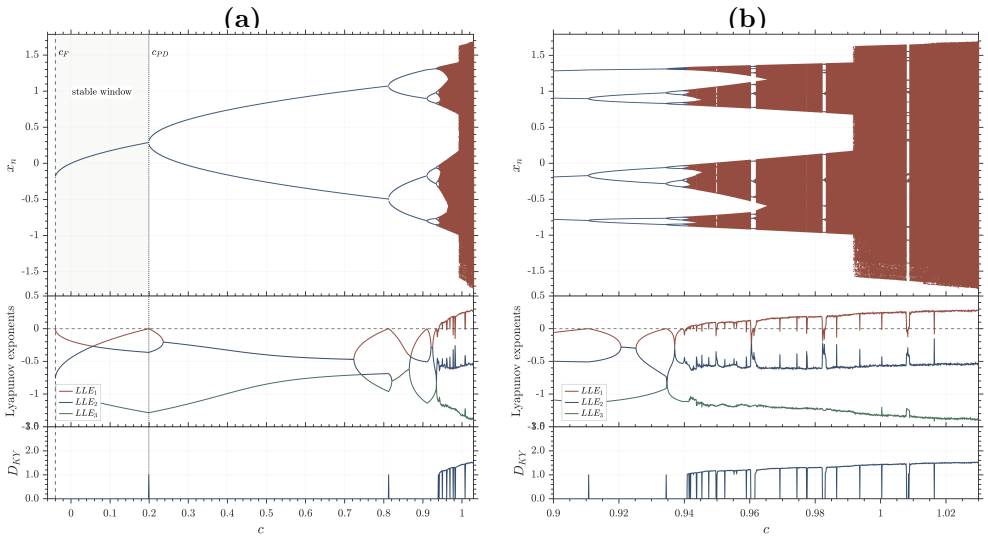


Fig. 1 One-parameter continuation for $(k, \eta, \mu) = (0.35, 0.25, 0.45)$. Panel (a) shows the attracting branch and its post-flip dynamics for $-0.06 \leq c \leq 1.03$, together with the Lyapunov spectrum and Kaplan–Yorke dimension. The analytical thresholds are $c_F = -0.04$ and $c_{PD} = 0.19883714880333$. Panel (b) magnifies $0.9 \leq c \leq 1.03$, where chaotic bands are interrupted by periodic windows. The computations used $N_{\text{trans}} = 6000$, $N_{\text{keep}} = 2400$ for panel (a), and $N_{\text{trans}} = 7000$, $N_{\text{keep}} = 2600$ for panel (b).

branch can lose stability only through the real multiplier -1, provided that the flip genericity conditions in Proposition 10 hold.

Figure 1(a) illustrates this real-multiplier scenario. The attracting upper branch is created after the fold at $c = c_F$ and remains stable until the flip threshold $c = c_{PD}$. Beyond this point, the loss of stability is expressed by a period-doubling route, where the attracting fixed point is replaced by attracting periodic orbits, and further doublings lead to chaotic bands. The Lyapunov spectrum records this transition. All exponents are negative in the stable fixed-point and periodic regimes, whereas a positive leading exponent marks the intervals where the selected bounded orbit is chaotic. The Kaplan–Yorke dimension is therefore not an independent bifurcation detector, but a compact summary of the Lyapunov spectrum: it is zero on attracting fixed points and periodic orbits and becomes noninteger when the leading Lyapunov exponent is positive.

The zoomed view in Figure 1(b) shows that the post-flip region is organized by alternating regular and chaotic time intervals. The chaotic bands are interrupted by narrow, attracting periodic windows. These windows appear simultaneously as contractions of the point cloud in the bifurcation diagram, downward dips of the leading Lyapunov exponent, and drops in D_{KY}. Thus, the local flip threshold explains the first destabilization, whereas the subsequent band splitting and periodic windows reflect the global return geometry of the delayed filtered-memory map. In this sense, post-critical dynamics are not determined solely by the local multiplier crossing; they are shaped by the repeated action of quadratic folding, the delay coordinate, and the recursive filter.

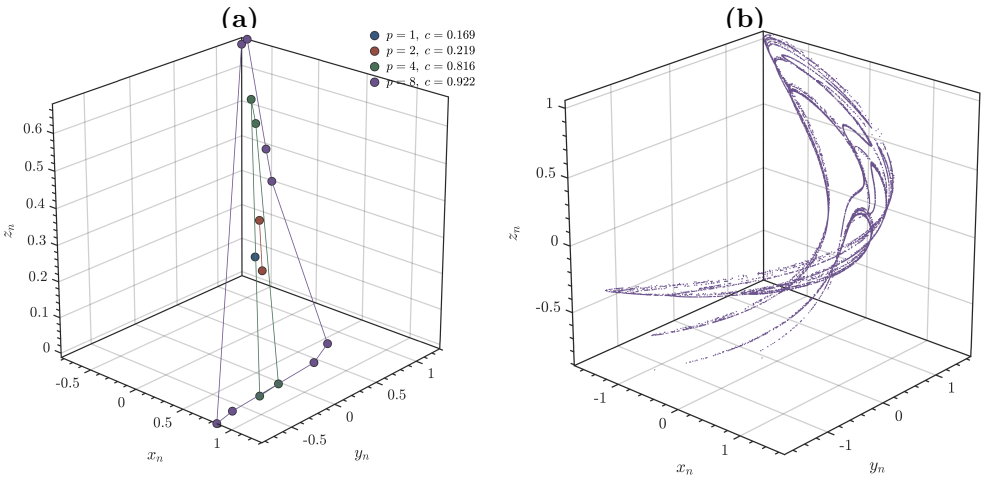


Fig. 2 Representative attractors in the embedded delay–memory phase space (x_n, y_n, z_n) for $(k, \eta, \mu) = (0.35, 0.25, 0.45)$. Panel(a) shows the attracting periodic orbits with $p = 1$ at $c = 0.169$, $p = 2$ at $c = 0.219$, $p = 4$ at $c = 0.816$, and $p = 8$ at $c = 0.922$. Panel (b) shows a chaotic attracting set at $c = 1.033$, with $LE_1 \approx 0.2791$.

The phase-space projections in Figure 2 show how the real-multiplier route is represented in the embedded delay–memory space. The period-one, period-two, period-four, and period-eight attractors appear as finite point sets, as expected after successive period doubling. Each plotted point represents a triple (x_n, x_{n-1}, z_n). Thus, the point clouds in this projection carry information on the present state, one-step-delayed state, and filtered record accumulated by the memory variable.

For the chaotic orbit in Figure 2(b), the finite periodic set opens into a folded cloud in embedded space. The shape comes from the three components of the map acting simultaneously: the quadratic term stretches and folds the x-coordinate, the delay coordinate records x_{n-1}, and the filter updates z_n as a smoothed memory of recent states. This is why the three-dimensional projection is useful here; it shows how the delayed and filtered variables participate in the geometry of the attracting sets.

This period-doubling route corresponds to the crossing of a real multiplier. Changing the sign and magnitude of the filtered-memory feedback provides another local scenario because the complex pair boundary can then become admissible. Figure 3 illustrates this situation for $(k, \eta, \mu) = (0.30, -2.31235, 0.65)$. For these parameters, Proposition 11 allows a non-real unit-circle pair, whereas the remaining real multiplier remains inside the unit disk. The diagnostic $|\lambda_{1,2}| - 1$ crosses zero at the predicted candidate value $c = c_C$, indicating that the relevant loss of stability is associated with a complex pair rather than the real multiplier -1.

The phase portraits in Figure 3(b) should be read with respect to the period-doubling panels in Figure 2. Here, the orbit does not separate into a finite 2^m-cycle. The retained points instead lie on closed curve-like sets, which is the expected numerical trace of a rotating complex pair near the unit circle. For the plotted parameters, the curves shrink as c approaches c_C, whereas the leading finite-time Lyapunov exponent remains close to zero. This behavior is consistent with a complex-pair mechanism:

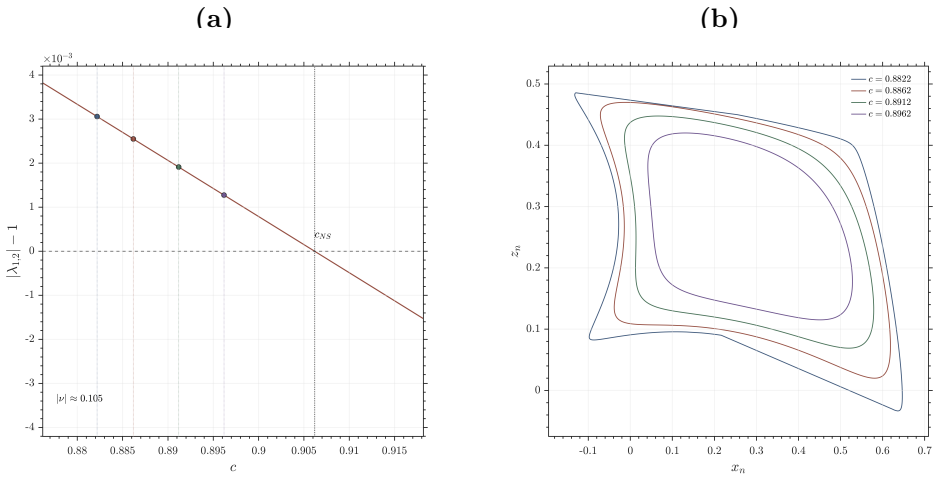


Fig. 3 Admissible complex-pair route for $(k, \eta, \mu) = (0.30, -2.31235, 0.65)$. Panel(a) shows the radial crossing diagnostic $|\lambda_{1,2}| - 1$ for the complex-conjugate fixed-point multipliers. The crossing occurs at $c_C = 0.906184473979591$, and the noncritical real multiplier satisfies $|\nu| \approx 0.105$. Panel (b) shows invariant curves for $c = 0.8822$, 0.8862, 0.8912, and 0.8962.

the local motion is governed by a rotating two-dimensional center direction, not by the one-dimensional flip direction. Therefore, the closed curves in Figure 3(b) are used here as numerical evidence of the admissible complex pair route. Their role is to illustrate the local post-critical geometry near the complex-pair boundary.

Figures 1–2 and Figure 3 show two different ways in which the stable fixed point can lose stability. With positive filtered feedback, the route passes through the real multiplier -1, and the computed orbit develops by period-doubling. When the filtered feedback is sufficiently negative, the complex pair boundary becomes accessible, and the nearby orbit has a rotational curve-like form. This change is produced by the memory variable through the multiplier conditions of the embedded maps.

Figure 4 places the one-parameter observations in a broader parameter context. The superimposed analytical curves locate the local fixed-point thresholds: the fold curve gives the birth or disappearance of real fixed points, the flip curve gives the real-multiplier loss of stability, and the admissible complex-pair curve selects the part of the third Schur–Jury boundary where a non-real unit-circle pair is possible. The color does not add another analytical threshold; it records the largest finite-time Lyapunov exponent of the orbit selected using the numerical protocol. Negative values corresponded to attracting fixed or periodic responses, positive values to chaotic responses, and white regions to escape or incomplete diagnostics.

The (η, c)-plane clearly shows how the sign of the filtered feedback changes the available route. For positive η, the relevant stability loss follows the fold–flip scenario: the fixed point is created at the fold curve and later destabilizes through the flip curve. As η decreases through negative values, the admissible complex pair curve enters the same region of the scan. This is the numerical counterpart of Proposition 11: changing

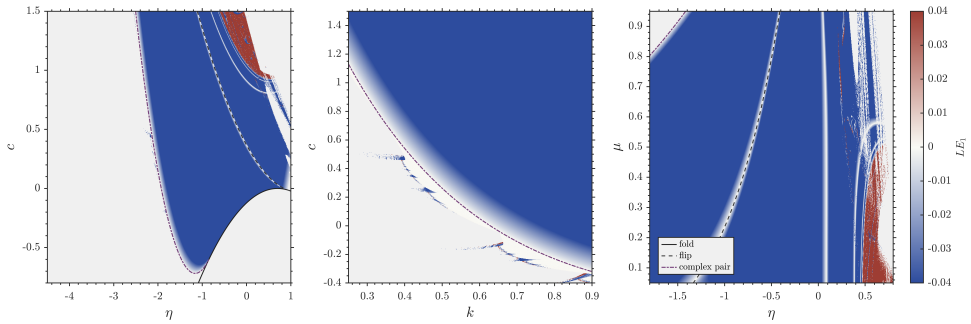


Fig. 4 Selected two-parameter Lyapunov maps. The left, middle, and right panels show the (η, c)-, (k, c)-, and (η, μ)-planes, respectively. The color represents the largest finite-time Lyapunov exponent LE_1, clipped to $[-0.04, 0.04]$. The white regions correspond to the escaping or invalid trajectories for the tested initial conditions. The solid, dashed, and dash-dotted curves denote the fold, flip, and admissible complex pair boundaries, respectively. The final scans used $N_{\mathrm{grid}} = 800$, $N_{\mathrm{trans}} = 8500$, $N_{\mathrm{keep}} = 3500$, parallel computation, and no display smoothing.

the filtered feedback can move the system from a real-multiplier route to a complex pair route.

In the (k, c)-plane, varying the delayed-feedback coefficient changes both the fixed-point thresholds and the volume factor $\det DF = -k(1 - \mu)$. The fold curve tracks where the real fixed-point branch is born, whereas the flip curve indicates where the stable upper branch can lose stability through the multiplier -1. The color changes around this curve indicate a transition from attracting fixed or periodic behaviors to post-flip dynamics. Because the scan follows a selected initial condition and a finite-time Lyapunov average, the colored regions should be interpreted as the observed attracting response along this numerical protocol and not as a full global description.

In the (η, μ)-plane, the distinction between the fixed-point location and the multiplier structure becomes explicit. The parameter μ does not enter the fixed-point equation, but it enters the Jacobian, and therefore shifts the stability and admissibility boundaries. Consequently, changes in μ can alter the observed Lyapunov response, even when the algebraic fixed-point branch is not moved directly. This panel illustrates the main structural effect of recursive memory: the memory update rate modifies stability through multipliers rather than through the fixed-point position.

The white regions in Figure 4 indicate parameter values for which the selected orbit exceeded the numerical escape threshold or for which the finite-time diagnostics were incomplete. Hence, the scans show the attracting response selected by the continuation procedure rather than a full global description of all attracting responses.

Overall, the numerical experiments support the analytical separation between the real-multiplier and complex-pair routes. In the positive delay–filter regime, the upper fixed-point branch loses stability through the flip threshold and gives rise to a period-doubling route with periodic windows and chaotic bands. When the feedback signs allow the third Schur–Jury boundary to become admissible as a complex-pair crossing,

the post-critical dynamics changes toward invariant-curve-like behavior. The filtered-memory parameters therefore do not merely shift numerical diagrams; they determine which unit-circle mechanism becomes dynamically accessible.

6 Conclusion

Starting from the literature on memory-modified logistic and quadratic maps, we examined a delayed quadratic recurrence with recursive filtered-memory feedback. The recurrence was rewritten as a smooth three-dimensional polynomial map so that the delayed coordinate and filtered-memory state became explicit components of the phase space. This embedding reveals a useful separation of roles among parameters. The delay strength k and filtered-memory strength η determine the fixed-point branch through the combined feedback term $k + \eta$, whereas the memory update rate μ does not affect the fixed points. Its effect appears in the Jacobian, where it changes the multiplier structure. In this sense, recursive filtered memory modifies stability through local linearization rather than through the algebraic fixed-point equation.

The fixed-point stability problem was reduced to explicit Schur–Jury inequalities in the coordinate x^*. From this reduction, the real-multiplier thresholds were obtained in closed form and interpreted as fold and flip boundaries, respectively, under explicit genericity conditions. The equality $\eta = (2 - \mu)(1 - k)$ marks the coincidence of these two thresholds and hence defines the fold–flip degeneracy of the fixed-point structure. A separate conclusion concerns the third Schur–Jury equality. It cannot be identified automatically with a Neimark–Sacker bifurcation; it is only a complex-pair candidate boundary. It becomes admissible as a non-real unit-circle crossing only under sign-dependent conditions for the filtered-memory feedback. Thus, the central question raised in the introduction is answered explicitly: delay and filtered memory do not simply shift the stability window but determine which unit-circle route is accessible from a stable fixed point.

Simulations were used to dynamically read the analytical thresholds. In the positive delay–filter regime, the admissible route is a real-multiplier one: the upper fixed-point branch loses stability at the flip threshold, after which the computed orbit follows a period-doubling scenario with periodic windows and chaotic bands. The local geometry changes when the signs of the feedback terms render the complex pair boundary admissible. The nearby post-critical motion is then organized by invariant-curve-like sets rather than by finite period-doubled orbits. These numerical observations support the main structural point of the study: the filtered-memory state is not just an additional coordinate but a mechanism that changes the multiplier geometry of the embedded quadratic map.

Several aspects remain outside the scope of this study. The bifurcation results are local and concern fixed points along one-parameter continuations in c, with k, η, and μ being held fixed. Therefore, they do not provide a complete unfolding in the full parameter space. The fold–flip relation $\eta = (2 - \mu)(1 - k)$ has been identified as a degeneracy of thresholds; however, its two-parameter normal form has not been developed. Similarly, the invariant-curve-like behavior near the admissible complex-pair route has been supported numerically, but resonance tongues, mode locking, and

invariant-curve breakdown have not yet been analyzed. Parameter plane scans should also be understood as finite-time diagnostics for selected initial conditions and not as a complete global classification of all attracting responses.

These limitations point to several natural extensions of this work. One direction is to construct a two-parameter unfolding near the fold–flip degeneracy and examine possible interactions between the real-multiplier and complex-pair thresholds. Another is to compute the Neimark–Sacker normal-form coefficient systematically, so that supercritical and subcritical invariant-curve scenarios can be distinguished. The admissible complex-pair regime also invites a closer study of resonances, mode locking, and the breakdown of invariant curves. Globally, analytical estimates of boundedness and escape can be combined with multi-initial-condition simulations to study the organization of the attracting sets. Such developments would extend the present local theory toward a fuller description of the global dynamics generated by the recursive filtered memory in delayed quadratic maps.

Declarations

Funding

This research was supported by Universitas Diponegoro through the Non-State Budget Funding Scheme (Dana Selain APBN) for the Fiscal Year 2026. The support was provided under the Decree of the Head of the Institute for Research and Community Service (LPPM), Universitas Diponegoro, No. 8/UN7.A/HK/V/2026 dated May 5, 2026 and Contract Agreement No. 306-155/UN7.D2/PP/V/2026 dated May 5, 2026.

Conflict of interest

The authors declare no conflicts of interest.

Ethics approval and consent to participate

Not applicable.

Consent for publication

Not applicable.

Data availability

The data generated and analyzed during the numerical simulations are available from the corresponding author upon reasonable requests.

Materials availability

Not applicable.

Code availability

The code used to generate the numerical results and figures is available from corresponding author upon reasonable request.

Author contribution

Hafidh Khoerul Fata contributed to the conceptualization, model formulation, analytical derivations, numerical simulations, visualization, and writing of original manuscript. Yosephus Decupertino Sumanto contributed to the mathematical validation, interpretation of results, and manuscript review. Robertus Heri Soelistyo Utomo contributed to the validation of the analysis, discussion of the numerical results and manuscript review. All authors read and approved the final manuscript.

References

[1] May, R.M.: Simple mathematical models with very complicated dynamics. Nature **261**, 459–467 (1976) https://doi.org/10.1038/261459a0

[2] Gallas, J.A.C.: Simulating memory effects with discrete dynamical systems. Physica A: Statistical Mechanics and its Applications **195**(3–4), 417–430 (1993) https://doi.org/10.1016/0378-4371(93)90167-3

[3] Dehghan, M., Kent, C.M., Mazrooei-Sebdani, R., Ortiz, N.L., Sedaghat, H.: Dynamics of rational difference equations containing quadratic terms. Journal of Difference Equations and Applications **14**(2), 191–208 (2008) https://doi.org/10.1080/10236190701565636

[4] Bektešević, J., Kulenović, M.R.S., Pilav, E.: Global dynamics of quadratic second order difference equation in the first quadrant. Applied Mathematics and Computation **227**, 50–65 (2014) https://doi.org/10.1016/j.amc.2013.10.048

[5] Saleh, M., Herzallah, S.: Dynamics and bifurcation of a second order rational difference equation with quadratic terms. Journal of Applied Nonlinear Dynamics **10**(3), 563–578 (2021) https://doi.org/10.5890/JAND.2021.09.014

[6] Zhong, J., Deng, S.: Two codimension-two bifurcations of a second-order difference equation from macroeconomics. Discrete and Continuous Dynamical Systems - Series B **23**(4), 1581–1600 (2018) https://doi.org/10.3934/dcdsb.2018062

[7] Holopainen, R.: Logistic map with a first order filter. International Journal of Bifurcation and Chaos **21**(6), 1773–1781 (2011) https://doi.org/10.1142/S0218127411029422

[8] Alonso-Sanz, R.: Extending the parameter interval in the logistic map with memory. International Journal of Bifurcation and Chaos **21**(1), 101–111 (2011) https://doi.org/10.1142/S0218127411028052

[9] Alonso-Sanz, R., Losada, J.C., Porras, M.A.: Bifurcation and chaos in the logistic map with memory. International Journal of Bifurcation and Chaos **27**(12), 1750190 (2017) https://doi.org/10.1142/S0218127417501905

[10] Góra, P., Boyarsky, A., Li, Z., Proppe, H.: Statistical and deterministic dynamics of maps with memory. Discrete and Continuous Dynamical Systems - Series A **37**(7), 3755–3774 (2017) https://doi.org/10.3934/dcds.2017186

[11] Stanislavsky, A.A.: Long-term memory contribution as applied to the motion of discrete dynamical systems. Chaos **16**(4), 043105 (2006) https://doi.org/10.1063/1.2358632

[12] Tarasov, V.E.: Discrete map with memory from fractional differential equation of arbitrary positive order. Journal of Mathematical Physics **50**(12), 122703 (2009) https://doi.org/10.1063/1.3272791

[13] Levin, S.A., May, R.M.: A note on difference-delay equations. Theoretical Population Biology **9**(2), 178–187 (1976) https://doi.org/10.1016/0040-5809(76)90043-5

[14] Samuelson, P.A.: Interactions between the multiplier analysis and the principle of acceleration. The Review of Economic Statistics **21**(2), 75–78 (1939) https://doi.org/10.2307/1927061

[15] Bischi, G.I.: From samuelson's multiplier-accelerator to bifurcations and chaos in economic dynamics. Decisions in Economics and Finance **48**, 2193–2214 (2025) https://doi.org/10.1007/s10203-024-00462-0

[16] Pyragas, K.: Continuous control of chaos by self-controlling feedback. Physics Letters A **170**(6), 421–428 (1992) https://doi.org/10.1016/0375-9601(92)90745-8

[17] Boccaletti, S., Grebogi, C., Lai, Y.-C., Mancini, H., Maza, D.: The control of chaos: Theory and applications. Physics Reports **329**(3), 103–197 (2000) https://doi.org/10.1016/S0370-1573(99)00096-4

[18] Kuznetsov, Y.A., Meijer, H.G.E.: Numerical normal forms for codim 2 bifurcations of fixed points with at most two critical eigenvalues. SIAM Journal on Scientific Computing **26**(6), 1932–1954 (2005) https://doi.org/10.1137/030601508

[19] Hu, D., Liu, X., Li, K., Liu, M., Yu, X.: Codimension-two bifurcations of a simplified discrete-time SIR model with nonlinear incidence and recovery rates. Mathematics **11**(19), 4142 (2023) https://doi.org/10.3390/math11194142

[20] Niu, W., Shi, J., Mou, C.: Analysis of codimension 2 bifurcations for high-dimensional discrete systems using symbolic computation methods. Applied Mathematics and Computation **273**, 934–947 (2016) https://doi.org/10.1016/j.amc.2015.10.009

[21] Dutta, D., Bhattacharjee, J.K.: Period adding bifurcation in a logistic map with memory. Physica D: Nonlinear Phenomena **237**(24), 3153–3158 (2008) https://doi.org/10.1016/j.physd.2008.05.014

[22] Shimada, I., Nagashima, T.: A numerical approach to ergodic problem of dissipative dynamical systems. Progress of Theoretical Physics **61**(6), 1605–1616 (1979) https://doi.org/10.1143/PTP.61.1605

[23] Benettin, G., Galgani, L., Giorgilli, A., Strelcyn, J.-M.: Lyapunov characteristic exponents for smooth dynamical systems and for hamiltonian systems; a method for computing all of them. part 1: Theory. Meccanica **15**(1), 9–20 (1980) https://doi.org/10.1007/BF02128236

[24] Wolf, A., Swift, J.B., Swinney, H.L., Vastano, J.A.: Determining lyapunov exponents from a time series. Physica D: Nonlinear Phenomena **16**(3), 285–317 (1985) https://doi.org/10.1016/0167-2789(85)90011-9

[25] Kaplan, J.L., Yorke, J.A.: Chaotic behavior of multidimensional difference equations. In: Peitgen, H.-O., Walther, H.-O. (eds.) Functional Differential Equations and Approximation of Fixed Points. Lecture Notes in Mathematics, vol. 730, pp. 204–227. Springer, Berlin (1979). https://doi.org/10.1007/BFb0064319